



Article

The Water Hammer Characteristics of Long-Distance Water Pipelines under Different Water Supply Modes

Yongzhi Wang ¹, Tao Wang ¹, Yunlong Ran ², Xiaolei Zhang ^{3,*}, Xiaoyi Guo ³  and Shuyu Liu ^{3,4} ¹ Henan Water Diversion Engineering Co., Ltd., Zhengzhou 450003, China² Henan Water Valley Innovation Technology Research Institute Co., Ltd., Zhengzhou 450046, China; nkym0902@163.com³ School of Water Conservancy, North China University of Water Resources and Electric Power, Zhengzhou 450046, China; declaral1900@163.com (X.G.)⁴ College of Water Conservancy and Hydropower Engineering, Hohai University, Nanjing 210098, China

* Correspondence: zhangxiaolei@ncwu.edu.cn

Abstract: The pressure characteristics of long-distance water pipelines during hydraulic transient processes are crucial for ensuring the safe, stable, and long-term operation of water transfer projects. This paper establishes a one-dimensional mathematical model based on sections of the Yinjiangjihuai long-distance water diversion project in China. The water supply requirements of the pipelines are categorized into two replenishment modes as follows: gravity supply and pump-pressurized water supply. The opening and closing strategies of the water pipelines under different flow conditions are simulated and analyzed to explore the hydraulic transient processes under various water supply modes. The transient variations of key hydraulic parameters during valve closure are clarified. Simulation results indicate that the water pipeline design is reasonable, meeting the water supply demands at relatively low Manning values and that it has the capability for long-term supply. Due to the excessive head provided by the pumps, pump-pressurized water supply and gravity supply modes cannot operate simultaneously. Under gravity supply mode, the minimum pressure in the downstream pipeline is relatively higher overall, while the maximum pressure in the upstream pipeline is relatively lower overall. In the pump-pressurized water supply mode, the safety and stability of the water supply can be ensured by adjusting the closing time of individual pumps and the interval time between adjacent pumps. The research findings provide technical guidance and scientific basis for the construction of national water networks and water transfer projects.

Keywords: gravity flow; pump-pressurized water supply; method of characteristics; one-dimensional mathematical model; water hammer



Citation: Wang, Y.; Wang, T.; Ran, Y.; Zhang, X.; Guo, X.; Liu, S. The Water Hammer Characteristics of Long-Distance Water Pipelines under Different Water Supply Modes. *Water* **2024**, *16*, 2008. <https://doi.org/10.3390/w16142008>

Academic Editors: Chin H Wu and Giuseppe Pezzinga

Received: 12 June 2024

Revised: 2 July 2024

Accepted: 10 July 2024

Published: 15 July 2024



Copyright: © 2024 by the authors. Licensee MDPI, Basel, Switzerland. This article is an open access article distributed under the terms and conditions of the Creative Commons Attribution (CC BY) license (<https://creativecommons.org/licenses/by/4.0/>).

1. Introduction

Long-distance water conveyance projects play a crucial role in providing drinking water to urban and rural residents, agricultural irrigation, and industrial production support due to their characteristics of cross-regional coverage, large scale, stable transmission, and strong anti-pollution capability [1–3]. However, during hydraulic transients, problems such as pressure fluctuations, cavitation, and water hammer effects are common [4,5], and issues like corrosion, leakage, blockage, and pipe bursts still need to be prevented [6–9]. These problems seriously affect the safety and stability of water conveyance systems. To mitigate these impacts, researchers have proposed various solutions and calculation methods.

The study of water hammer phenomena began in the early 19th century. Through the study of wave propagation theory, Joukowski derived the most famous basic equation of water hammer [10]. The Method of Characteristics (MOC), Finite Volume Method (FVM), Lattice Boltzmann Method (LBM), Smoothed Particle Hydrodynamics (SPH), and Preissmann slot method have been widely applied in water hammer analysis. The FVM, with its numerical stability and wide applicability, plays an important role in the simulation

of long-distance pipelines. However, the FVM also has high computational complexity, especially when dealing with complex boundary conditions and nonlinear problems [4]. The LBM is notable for its ability to handle complex boundary conditions and its parallel computing advantages. Despite significant progress in water hammer analysis, challenges remain in terms of computational complexity and numerical stability [11]. The SPH method excels in handling free-surface flows and multiphase flows, but it may face numerical dissipation and stability issues in high Reynolds number flows [5]. The Preissmann slot method simplifies the simulation of free-surface flows by introducing the slot concept, but it may have limitations when dealing with complex geometries and high-velocity conditions [12].

In recent years, one-dimensional mathematical models based on the Method of Characteristics (MOC) have been extensively applied in hydraulic transient calculations for various water pipelines. For instance, they have been utilized to investigate the effects of the opening and closing of ultra-supercritical steam traps on the temporal curves of pipeline flow and water hammer pressure [13], as well as the protection of water pipelines by air valve groups to mitigate water hammer effects [14], and the fluctuation of hydraulic parameters such as elastic modulus and Poisson's ratio in different pipelines [15]. Concurrently, significant progress has been made in optimizing the Method of Characteristics. For example, Hwang [16] introduced shock particles with dual states to enhance the accuracy of pipeline simulations; Liang et al. [17] established a systematic water hammer protection model based on wave characteristic methods and conducted numerical simulation analyses under different water hammer conditions. The Method of Characteristics can also be coupled with other methods for solution. In one-dimensional coupled mathematical models, Wang et al. [18] combined the Method of Characteristics (MOC) with the Method of Implicit (MOI) to simulate non-steady flow and hydraulic transient processes in pipelines; in one-dimensional coupled with two-dimensional mathematical models, Riasi et al. [19] used modified implicit characteristic methods to solve the quasi-two-dimensional equations of transient flow in pipelines; and in one-dimensional coupled with three-dimensional mathematical models, Geng et al. [20] combined the one-dimensional Method of Characteristics (MOC) with the three-dimensional Finite Volume Method (FVM) to simulate pressure fluctuations driven by water hammer.

The water pipelines ensure safe passage through hydraulic transient processes by implementing operational strategies and additional protective measures. The opening and closing strategy for water pipelines should comprehensively consider the sequence of pump or valve closure, the initial valve opening degree, and the opening and closing speed [21–23]. The aim is to prevent water hammer waves generated by the opening and closing of branch valves or pumps from superimposing on the main pipeline, thereby avoiding increased pressure or the generation of large amounts of gas. Additionally, water pipelines can mitigate peak values of hydraulic parameters during fluctuation processes by installing air valves, pressure relief valves, pressure regulating wells, and other measures [24–26]. Among these, air valves ensure the safe and stable operation of water pipelines by separating gas and liquid, adjusting pressure, and preventing water hammer. Wang et al. [27] formulated air valve placement standards based on the analysis of pipeline burst events to reduce the risk of secondary bursts; Li et al. [28,29] studied the effects of air valve types, orifice diameters, and discharge coefficients on water column separation and water hammer protection. Although the aforementioned scholars have conducted research on various types and placement methods of air valves and other protective measures, the deployment of air valves and similar protective measures can also be obtained through learning algorithms. Bostan et al. [30] studied the optimization design of dampers and layout in water distribution systems based on genetic algorithms; Alhwij et al. [31] similarly explored the protective performance of pressure vessel size, orifice diameter, and air valve orifice diameter and discharge coefficient based on genetic algorithms.

Gravity and pressurized water supply are two modes of long-distance water conveyance projects. It is essential to study the hydraulic transient processes under both

supply modes. Therefore, this paper establishes a one-dimensional mathematical model based on the Method of Characteristics. It discusses the impact of air valve exhaust capacity on water hammer attenuation in conjunction with the valve-closing strategy for pressurized water supply, and further explores the optimal valve-closing strategies under different supply modes.

2. Mathematical Model

2.1. Water Conveyance Pipeline

The research object selected is the water conveyance pipeline from Qiliqiao Reservoir to Xiayi in the Yinjiangjihuai long-distance water diversion project in China, as shown in Figure 1. The designed water levels of the upstream and downstream reservoirs on the pipeline are 46.00 m and 39.00 m, respectively. Based on the water levels at the inlet and outlet of the pipeline, it is known that the pipeline can meet gravity flow water conveyance under low flow conditions, while pressurized water conveyance is required under high flow conditions.

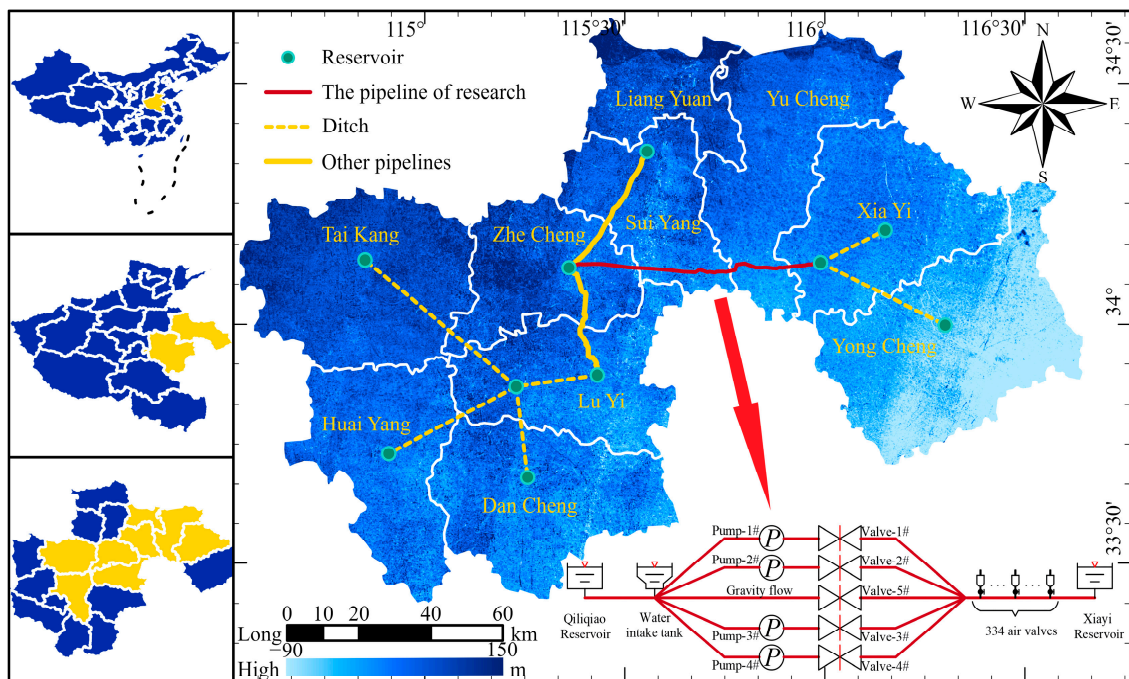


Figure 1. Study area and water conveyance pipeline structure. Created by ArcGIS 10.6 software (<https://www.arcgis.com>).

The water conveyance pipeline was constructed using a DN3200 PCCP (Prestressed Concrete Cylinder Pipe) for the water supply, with a design flow rate and pipeline length of $13.80 \text{ m}^3/\text{s}$ and 61.62 km , respectively. Additionally, 344 sets of air valves were installed to ensure water supply safety. The pressurized pumping station of the pipeline consists of four sets of pump units, operating in a three-in-one standby mode under design flow conditions. The rated head, flow rate, speed, and moment of inertia of the pumps are 35 m , $6.389 \text{ m}^3/\text{s}$, 425 rpm , and $340 \text{ kg}\cdot\text{m}^2$, respectively, while the moment of inertia of the motors is $1373 \text{ kg}\cdot\text{m}^2$. Furthermore, the water conveyance pipeline can still provide $5.60 \text{ m}^3/\text{s}$ of water even under conditions of gravity flow water supply only.

2.2. Basic Equations and Method of Characteristics

2.2.1. Basic Equations of Water Hammer

The Method of Characteristics is commonly applied in the modeling and analysis of water hammer in one-dimensional mathematical models for water conveyance pipelines. Compared to other methods, the Method of Characteristics offers advantages such as

numerical stability [32], wide applicability [33], fast solution speed [34], and high flexibility [20]. Considering the pressure head changes caused by water hammer, the basic equation of water hammer can be simplified into the following motion and continuity differential equations:

$$\frac{\partial Q}{\partial t} + gA \frac{\partial H}{\partial x} + \frac{fQ|Q|}{2DA} = 0 \tag{1}$$

$$gA \frac{\partial H}{\partial t} + a^2 \frac{\partial Q}{\partial x} = 0 \tag{2}$$

where Q represents the flow rate; H denotes the piezometric head; g is the local gravitational acceleration; A stands for the cross-sectional area of the pipe; f represents the friction coefficient of the pipe wall; D represents the diameter of the pipe; and a , x , and t , respectively, represent the wave speed of the water hammer, the distance of water hammer wave propagation, and time.

In the derivation of Equations (1) and (2), it is assumed that the flow is one-dimensional, incompressible, and quasi-steady in a rigid pipe. These assumptions simplify the complex nature of fluid dynamics to a more manageable form, suitable for long pipeline analysis. The linear friction factor represents viscous effects, and the equations consider a uniform cross-sectional area [35].

2.2.2. Method of Characteristics

By introducing a constant λ and multiplying it by Equation (2), then adding Equation (1), where $\lambda = \pm \frac{g}{c}$, the equations are simplified. Taking into account that both H and V are functions of x and t , and x is a function of t , a total derivative simplification analysis is conducted. Furthermore, by introducing the cross-sectional area of the pipeline (A), the flow rate (Q) replaces the flow velocity (V), leading to the positive and negative characteristic lines in the Method of Characteristics. Figure 2 displays the computational grid for the Method of Characteristics, with Equations (3) and (4) presenting the computational formulae for the positive and negative characteristic lines, respectively. Where P is the flux to be determined at the i -th node of the pipeline at the next moment, and A and B are the fluxes at the $(i - 1)$ -th and $(i + 1)$ -th nodes at the previous moment, respectively.

$$C^+ : H_P = C_A - S_A Q_P \tag{3}$$

$$C^- : H_P = C_B + S_B Q_P \tag{4}$$

where:

$$C_A = H_A + \frac{c}{gA} Q_A \tag{5}$$

$$S_A = \frac{c}{gA} + \frac{f\Delta x}{2gdA^2} |Q_A| \tag{6}$$

$$C_B = H_B - \frac{c}{gA} Q_B \tag{7}$$

$$S_B = \frac{c}{gA} + \frac{f\Delta x}{2gdA^2} |Q_B| \tag{8}$$

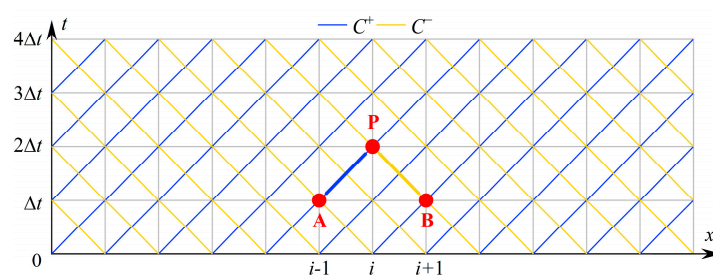


Figure 2. Computational grid.

2.2.3. Solution Equation of Air Valve

The air valves in the pipeline are designed to perform functions such as rapid air exhaust, high-speed air intake, air–water phase exhaust, and trace exhaust. Among them, the rapid intake and exhaust apertures have a diameter of DN100 mm, while the trace exhaust apertures have a diameter of DN5 mm. According to the basic principles of thermodynamics and fluid mechanics, the following four situations are delineated based on the absolute atmospheric pressure outside the pipeline (P_0) and the absolute pressure inside the pipeline (P) [36]:

- ① When air flows into the air valve at subsonic speed ($P_0 > P > 0.528P_0$):

$$\dot{m} = C_{in}A_{in}P_0\sqrt{\frac{7}{RT_0}\left[\left(\frac{P}{P_0}\right)^{1.4286} - \left(\frac{P}{P_0}\right)^{1.714}\right]} \quad (9)$$

- ② When air flows into the air valve at critical flow velocity ($P < 0.528P_0$):

$$\dot{m} = C_{in}A_{in}P_0\frac{0.686}{\sqrt{RT_0}} \quad (10)$$

- ③ When air is discharged from the air valve at subsonic speed ($1.894P_0 > P > P_0$):

$$\dot{m} = -C_{out}A_{out}P\sqrt{\frac{7}{RT}\left[\left(\frac{P_0}{P}\right)^{1.4286} - \left(\frac{P_0}{P}\right)^{1.714}\right]} \quad (11)$$

- ④ When the air valve flows out at critical velocity ($P > 1.894P_0$):

$$\dot{m} = -C_{out}A_{out}P\frac{0.686}{\sqrt{RT}} \quad (12)$$

where C_{in} and C_{out} represent the intake and exhaust flow coefficients of the air valve, respectively; A_{in} and A_{out} represent the cross-sectional areas of the intake and exhaust valves of the air valve, respectively; R is the gas constant; T is the absolute temperature inside the pipe; and T_0 is the absolute atmospheric temperature outside the pipe.

Combining the ideal gas equation, the Method of Characteristics equation, and the equation relating pressure and hydraulic head, the boundary condition equation for the air valve at the end of the time step is derived [28] as follows:

$$P\left\{V_i + 0.5dt\left[Q_{out} - Q_{in}\frac{C_A + C_B}{B} + \frac{2}{B}\left(\frac{P}{\rho g} + Z - H_0\right)\right]\right\} = [m_0 + 0.5dt(\dot{m}_0 + \dot{m})]RT \quad (13)$$

where ρ is the fluid density; V_i is the point volume at the beginning of the time step; Q_{in} and Q_{out} are the inflow and outflow rates at the beginning and end of the time step, respectively; m_0 is the initial mass of air in the cavity; \dot{m}_0 and \dot{m} are the inflow or outflow rates of air in the cavity at the beginning and end of the time step, respectively; Z is the height of the air valve above the reference plane; and H_0 is the local atmospheric pressure.

2.2.4. Solution Equations of the Pump

The hydraulic balance equation for the pump outlet valve is:

$$H_{P3} = H_{P2} - \frac{Q_P|Q_P|}{2C_v} \quad (14)$$

where H_{P3} and C_v are, respectively, the pressure head measured downstream of the valve section and the resistance coefficient of the valve.

The hydraulic balance equation for the pump is:

$$H_{P2} = H_{P1} + H_P \quad (15)$$

The equation of motion for the pump unit:

$$T = -I \frac{d\omega}{dt} \quad (16)$$

Introducing relative head h , relative flow rate v , relative speed a , and relative torque β , two equations are derived based on the above equations:

$$C_A - C_B - vQ_r(S_A + S_B) + H_r(a^2 + v^2)W_H(x) - \frac{v|v|\Delta H_0}{\tau^2} = 0 \quad (17)$$

$$(a^2 + v^2)W_B(x) + \beta_0 - C_T(a_0 - a) = 0 \quad (18)$$

where $W_H(x) = \frac{h}{a^2+v^2}$; $W_B(x) = \frac{\beta}{a^2+v^2}$; $x = \pi + \tan^{-1}(\frac{v}{a})$; $\beta_0 = \frac{T_0}{T_r}$; $C_T = \frac{2GD^2n^2}{365pr\Delta t}$; H_P is the pump head; Q_P is the pump flow rate; n is the pump speed; T is the pump torque; p is the pump power; GD^2 is the rotational inertia of the pump unit; ΔH_0 is the head loss of the control valve; and τ is the relative opening. Subscript '0' indicates initial value; subscript 'r' indicates rated value.

Equations (17) and (18) are solved using the Newton–Raphson iterative method, where $W_H(x)$ and $W_B(x)$ are obtained through linear interpolation based on the pump unit characteristic curves [37].

2.2.5. Solving Equations of the Valve

The relationship between the head of the valve and the flow characteristics is as follows [38]:

$$\Delta H = \frac{K(\tau)}{2gA_V^2} Q^2 \quad (19)$$

where A_V is the cross-sectional area of the valve in full open position; and $K(\tau)$ is the pressure loss coefficient at different openings of the valve, obtainable through interpolation from the pressure loss characteristic curve of the valve.

By solving Equations (1), (2), and (19) simultaneously, the flow rate through the regulating valve can be determined for different valve openings at any given moment, as well as the pressure heads upstream and downstream of the regulating valve.

2.3. Model Validation

A mathematical model identical to the physical model by Sha et al. [39] was established to validate the accuracy, feasibility, and applicability of the one-dimensional mathematical model. By comparing the maximum hydraulic head measured in the pipeline at different valve closure times with the maximum hydraulic head calculated by the model, the simulation results were verified against experimental data, as shown in Figure 3.

Quantitative analysis of experimental data and simulation results can be conducted using the Nash efficiency coefficient, calculated by the following formula [40]:

$$NSE = 1 - \frac{\sum_{i=1}^n (h_i - f_i)^2}{\sum_{i=1}^n (h_i - \bar{h})^2} \quad (20)$$

where h_i represents the experimental results; f_i represents the simulated results; \bar{h} is the mean value of the sample dataset; n is the number of data points in the sample; and i is the index of the data point in the sample.

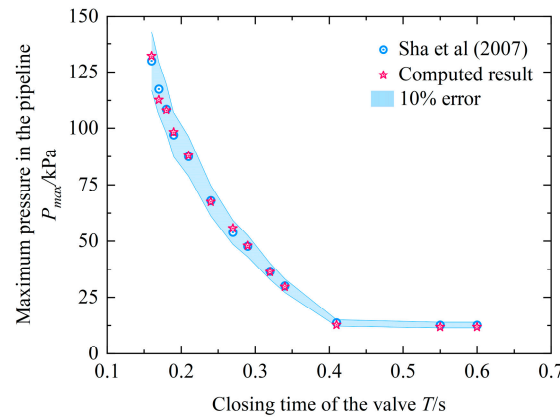


Figure 3. Comparison between simulation results and experimental data [39].

The Nash efficiency coefficient between the experimental data and simulated results is 0.92, indicating that the overall numerical simulation results closely match the average level of the measured data. This suggests a high credibility of the mathematical model and high accuracy of the simulation results. Furthermore, the error between the experimental data from Sha et al. [39] and the simulated results of the mathematical model is less than 10%, indicating precise control of the mathematical model parameters and appropriate selection of solution formulae, which accurately reflect the pressure fluctuations in pressurized pipelines.

3. Simulation Results Analysis

3.1. Analysis of Water Supply Modes for the Water Conveyance Pipeline

Due to the use of gravity flow for the water conveyance pipeline at low flow rates and pressurized flow at design standard flow rates, further exploration is required for the water supply mode of the pipeline system under other flow conditions. The pipeline’s centerline elevation and internal pressure under gravity flow and pressurized flow modes are shown in Figure 4.

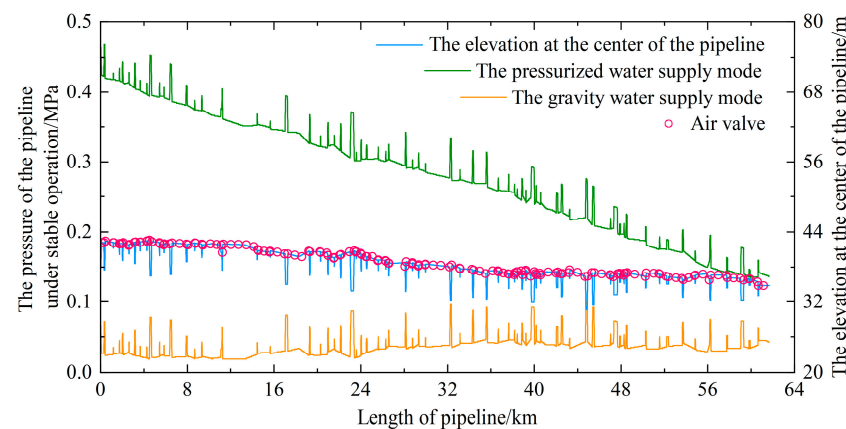


Figure 4. Pipeline centerline elevation and internal pressure.

Although there is a 7.0 m height difference between the upstream and downstream reservoirs of the water conveyance pipeline, the newly constructed pipeline system still has a surplus of 4.38 m and 13.97 m under gravity flow and pressurized flow modes, respectively. This indicates that the water conveyance pipeline initially possesses a certain stability for long-term water supply. Under long-term water supply conditions, the accumulation of deposits, scale, biofilm, and other pollutants on the inner wall of the pipeline will lead to a decrease in the Manning coefficient [41], further increasing the head loss along the pipeline. Under pressurized flow conditions, the water conveyance pipeline

can achieve the long-term water supply goal through the standby units of the pumping station. However, under gravity flow, without considering the actual flow diameter inside the pipeline, it will be unable to supply the rated flow when the Manning coefficient of the pipeline is less than 8.

Due to the design flow rates of $5.60 \text{ m}^3/\text{s}$ under gravity supply and $13.80 \text{ m}^3/\text{s}$ under pressurized supply for the pipeline, further investigation is required regarding whether a simultaneous supply mode of gravity and pressurized water should be adopted between these flow rates. Combining the rated head (35 m) and rated flow rate ($6.389 \text{ m}^3/\text{s}$) of the pump, the flow and head transformation process, as well as the pump efficiency curve, can be plotted as shown in Figure 5. The pump efficiency characteristics depicted in Figure 5 were generated using Hammer software (version 10.03), based on provided parameters including rated head, rated flow rate, rated speed, and the moment of inertia of the pump and motor. This figure is intended for preliminary simulation purposes to explore the feasibility of mixed gravity and pressurized water supply modes. Detailed analysis and accurate pump performance curves should be obtained from manufacturer specifications or empirical data for precise system design and analysis.

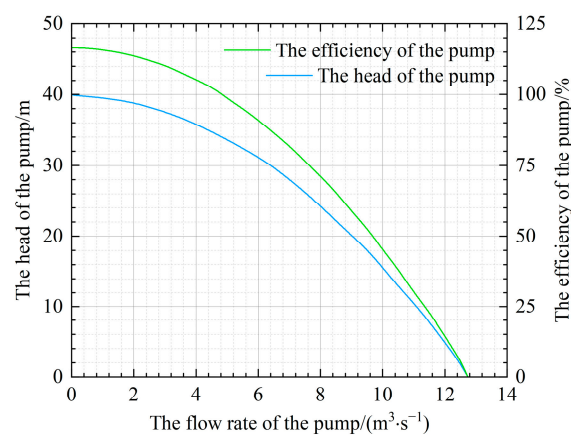


Figure 5. Pump water supply characteristics.

When the pipeline intends to achieve a larger flow rate (greater than $5.60 \text{ m}^3/\text{s}$ and less than $13.80 \text{ m}^3/\text{s}$) by using a single pump for pressurization in conjunction with gravity supply, according to China's "Design Standard for Pump Stations" (GB 50265-2022), the operating efficiency of a single pump should not be less than 80%. At this point, the head height of the pipeline connected to the single pump is much greater than 30 m. Referring to Figure 4, it can be observed that the downstream head height of the pipeline connected to gravity flow is only 4.59 m, significantly lower than that of the pipeline connected to the pump. Additionally, without the use of check valves, the pipeline connected to gravity flow will experience backflow.

3.2. Water Hammer Characteristics of Low Flow Supply

Combined with Figure 4, it can be seen that the elevation of the pipeline center overall decreases, with a height difference of 3.36 m between the upstream and downstream ends. Locally, the pipeline crosses rivers, roads, and other structures, forming a siphon-like pattern in the longitudinal direction, with a short-distance height difference reaching 6.886 m. Considering the wave speed of 750 m/s in the study pipeline segment, with a simulation time step of 0.005 s, the simulation time should be adjusted based on the pipeline length. The maximum adjustment should not exceed 25%, with an average adjustment of 3%.

In the gravity flow supply mode, the water supply pipeline achieves its supply objectives solely by opening and closing a single valve. Linearly closing the valve at 30, 60, and 90 s, the maximum pressure, minimum pressure along the pipeline, and gas volume (when

the pressure head of the pipeline drops to -10 m, water will vaporize, forming air [42]) are shown in Figure 6.

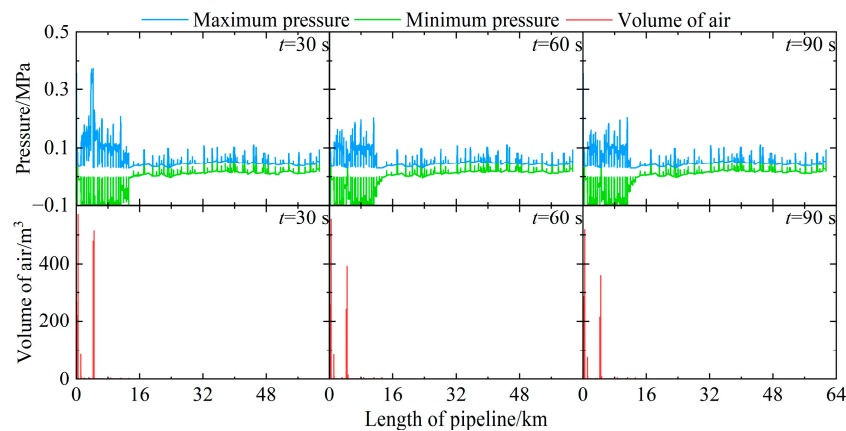


Figure 6. The maximum pressure, minimum pressure, and gas volume along the pipeline under gravity flow mode.

Combining the distribution of pipeline centerline elevation in Figure 4, it is observed that, disregarding the local inverted siphon pipeline, the centerline elevation of the upstream water supply pipeline (0~13.28 km) remains relatively constant, while that of the downstream water supply pipeline (13.28~61.62 km) shows a pronounced downward trend. When the valve at the upstream end of the water supply pipeline suddenly closes, water flow within the pipeline continues downstream under gravity. The downstream water supply pipeline not only replenishes and exhausts gases through pipeline outlets and air valves but also improves the efficiency of air valve utilization by adjusting gas density and pipeline elevation design. However, the small negative pressure generated in the upstream water supply pipeline after valve closure leads to gasification and the formation of gas, although the overall centerline elevation remains relatively flat. This condition suggests potential challenges in air valve operation in the upstream section compared to the downstream section, where the elevation changes more significantly. As a result, the efficiency of air valve utilization in the upstream water supply pipeline may vary due to these hydraulic differences.

Therefore, the air generated in the upstream water supply pipeline under valve closure is less likely to be expelled compared to the downstream pipeline, and the accumulation of gas easily induces the upstream water supply pipeline to experience flow cessation, exacerbating the complexity of the hydraulic transition process in the upstream pipeline. Adverse phenomena such as hydraulic fluctuations caused by water hammer become more pronounced with decreasing valve closure time. For instance, the maximum pressure in the water supply pipeline under valve closure times of 30, 60, and 90 s is 0.39, 0.37, and 0.36 MPa, respectively, while the maximum gas volume in the water supply pipeline under valve closure times of 30, 60, and 90 s is 570.6, 552.1, and 518.0 m³, respectively.

3.3. The Valve Closure Pattern for High-Flow Water Supply

The approach to water hammer protection for long-distance water pipelines mainly follows strategies such as reducing pipeline velocity, shortening the length of pressurized pipelines, and employing air valves as conventional hydraulic structures [17]. The water supply pipeline needs to adopt a centralized water supply to achieve high-flow water supply objectives. Moreover, considering the existing conditions of the water supply pipeline (without altering its length or introducing additional hydraulic structures), the protective measures that can be implemented are limited to reducing pipeline velocity.

Therefore, it is necessary to sequentially shut down the pumps to reduce the flow velocity of the water transmission pipeline in the pressurized water supply mode. Specifically, this is achieved by setting the individual pump shutdown time (t_1) and the interval time to

start shutting down the next pump (t_2). This study conducted numerical simulations with different combinations of $t_1 = 30, 60, 90$ s and $t_2 = 10, 20, 30$ s, and compared the maximum pressures along the pipeline under different scenarios. The design pressure of the water transmission pipeline is 0.6 MPa for the 0–30 km section and 0.4 MPa for the 30–61.62 km section. Figure 7a illustrates the maximum and minimum pressures along the pipeline under conditions of $t_1 = 30, 60$, and 90 s and $t_2 = 10$ s, while Figure 7b shows the maximum and minimum pressures along the pipeline under the condition of $t_1 = 30$ s and $t_2 = 10, 20$, and 30 s. The design pressure is multiplied by 1.5 to obtain the check pressure, as per the relevant design standards.

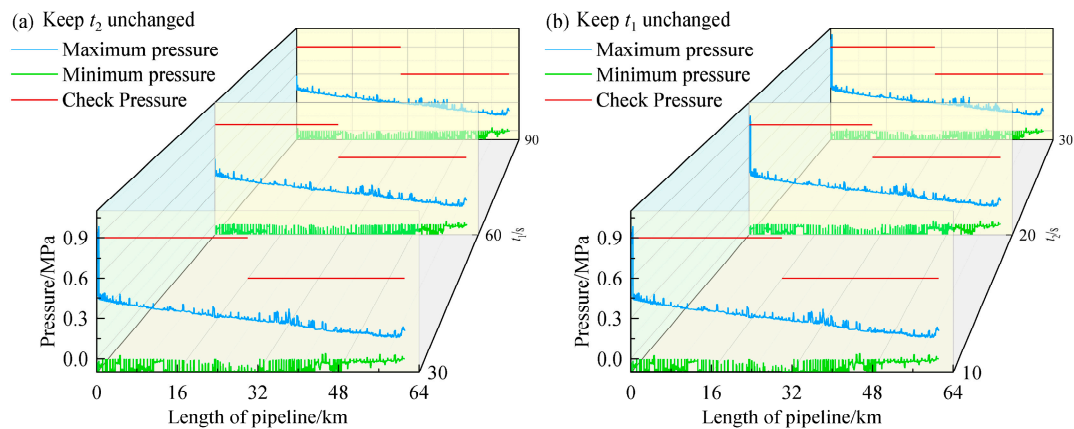


Figure 7. The maximum and minimum pressures under different conditions of t_1 and t_2 .

In Figure 7a, the water transmission pipeline experiences a maximum pressure exceeding the check pressure under the condition of $t_1 = 30$ s, specifically at a distance of 0.410 km where the maximum pressure reaches 1.04 MPa. The maximum pressures generated under the conditions of $t_1 = 60$ and 90 s are both less than the check pressure, with peak pressures along the pipeline of 0.588 MPa and 0.583 MPa, respectively. In Figure 7b, under the three valve-closing modes of $t_2 = 10, 20$, and 30 s, the water transmission pipeline produces maximum pressures exceeding the check pressure, measuring 1.04, 0.986 and 0.979 MPa, respectively. It can be observed that by extending the duration of t_2 to ensure stable hydraulic conditions during the hydraulic transition of the pipeline, followed by using a smaller t_1 to complete the final water cutoff, significant maximum pressures are generated. Considering the minimum pressures along the pipeline, it can be noted that the distribution of the minimum pressures along the pipeline is similar under the conditions of $t_1 = 60$ and 90 s. However, water vaporization due to a pressure head of -10 m reduces the effective flow area of the pipeline, leading to an increase in local flow velocity. This ultimately results in similar maximum pressures along the pipeline under the valve-closing mode of $t_2 = 10$ s and $t_1 = 60$ or 90 s.

Based on the above discussion, it can be inferred that the study can adopt a smaller valve-closing time ($t_1 = 30$ s) during the closing process of the first two pumps, while using a larger valve-closing time ($t_1 = 60$ s) for the final closing process, with a constant t_2 value of 10 s. Figure 8 illustrates the maximum and minimum pressures along the pipeline under this valve-closing method, along with the pressure, flow rate, and air fluctuation at the upstream node of the pipeline.

Under this valve-closing method, the maximum pressure along the pipeline remains consistently below the design pressure, meeting the requirements of the hydraulic transition process. The peak pressure along the pipeline is 0.588 MPa, which is equal to the peak pressure when all t_1 values were set to 60 s as mentioned earlier. The fluctuation patterns of pressure and flow rate at the upstream node of the pipeline (also the most critical node) are quite similar. The moments when the pressure, flow rate, and air reach their peaks at this node are approximately 160.45, 161.20, and 161.20 s, respectively. As the first valve closes completely, pressure and flow rate at the node begin to fluctuate, with

the fluctuation amplitude decreasing rapidly over a short period. When the second valve closes completely, pressure and flow rate at the node fluctuate again, with a longer duration and larger magnitude of fluctuations. Finally, when the third valve closes completely, the pressure fluctuation at the node reaches its minimum value, causing an increase in flow rate, and the longest time required for the amplitude of fluctuations to decrease.

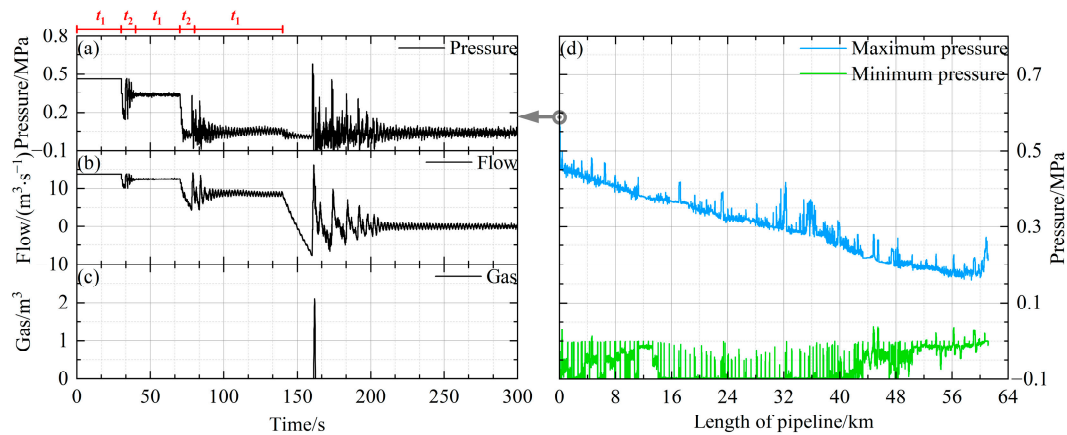


Figure 8. The pressure and hydraulic fluctuation characteristics along the water pipeline: (a) Variation in pressure at the upstream node; (b) Variation in flow rate at the upstream node; (c) Variation in gas composition at the upstream node; and (d) Maximum and minimum pressure along the pipeline.

4. Discussion

The simulation results provide significant insights into the hydraulic behavior of long-distance water pipelines under different water supply modes. Firstly, the study confirms the impossibility of simultaneous gravity and pumped flow operations due to the excessive head provided by the pumps. While this might seem an obvious conclusion, it underscores the necessity of thoroughly evaluating head requirements and operational constraints in water conveyance systems. This finding is crucial as it suggests that mixed flow scenarios require alternative design or operational strategies to avoid conflicts, which could impact the overall efficiency and safety of the water supply system.

Secondly, the analysis of valve closure times has revealed critical information about transient pressures within the pipeline. Shorter valve closure times were found to result in significantly higher transient pressures. For instance, a 30 s valve closure resulted in a maximum pressure of 0.39 MPa, whereas extending the closure time to 90 s reduced the maximum pressure to 0.36 MPa. This indicates the importance of optimizing valve operation strategies to manage water hammer effects effectively. By carefully controlling valve closure times, it is possible to mitigate the risks of excessive pressure surges, thereby enhancing the operational safety and reliability of the pipeline system.

The effectiveness of air valves in mitigating transient pressures was another key aspect of this study. The results showed that air valves play a crucial role in ensuring the safe operation of the pipeline by allowing controlled air intake and exhaust, thus reducing the impact of water hammer. However, the study also highlighted variations in the efficiency of air valve operation along the pipeline, influenced by local hydraulic conditions. For example, upstream sections experienced challenges due to small negative pressures leading to gasification. This suggests that strategic placement and appropriate sizing of air valves are essential to optimize their performance and ensure system stability.

Taking the air valve at the upstream location as an example, Figure 9 depicts the fluctuation of hydraulic parameters of the air valve under the aforementioned valve closure modes. According to the image, it can be observed that the air valve achieves and maintains a high exhaust capacity under both valve closure modes, and it is difficult to achieve better hydraulic conditions even with longer valve closure times. Therefore, this objective can be achieved through other hydraulic structures, such as pressure regulating wells [24,25].

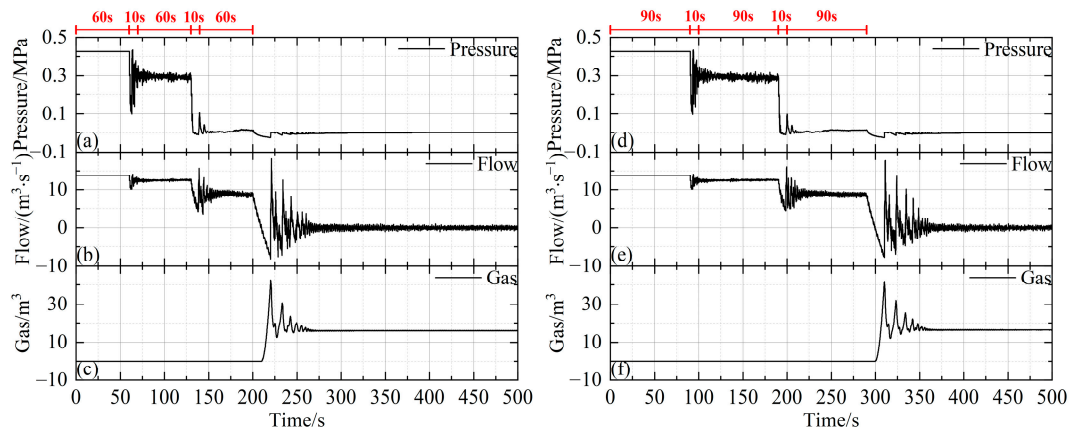


Figure 9. The hydraulic fluctuation of the air valve at the upstream end of the water pipeline. (a) Variation in pressure at the upstream air valve under valve closure conditions at 60 s; (b) Variation in flow rate at the upstream air valve under valve closure conditions at 60 s; (c) Variation in gas composition at the upstream air valve under valve closure conditions at 60 s; (d) Variation in pressure at the upstream air valve under valve closure conditions at 90 s; (e) Variation in flow rate at the upstream air valve under valve closure conditions at 90 s; and (f) Variation in gas composition at the upstream air valve under valve closure conditions at 90 s.

To support these findings, several studies have demonstrated similar conclusions regarding the importance of optimized valve closure strategies and the critical role of air valves. For example, Hwang et al. [16] emphasized the effectiveness of optimized valve operations in mitigating transient pressures. Similarly, Li et al. [28] highlighted the importance of strategic air valve placement to enhance system stability under transient conditions. Additionally, Pan et al. [5] demonstrated that the integration of multiple protective measures, including air valves and pressure regulating wells, is essential for comprehensive water hammer management in long-distance pipelines.

In light of these findings, several recommendations for the design and operation of long-distance water pipelines can be made. Optimized valve closure strategies should be implemented to manage transient pressures effectively, with longer closure times being preferable where feasible. Additionally, careful consideration must be given to the placement and sizing of air valves, particularly in sections with significant elevation changes or where negative pressures are likely to occur. Lastly, given the limitations of simultaneous gravity and pumped flow operations, it is recommended to explore alternative operational strategies such as sequential pumping or the use of backup pumps during high flow conditions.

5. Conclusions

This study relies on actual water supply engineering and establishes a one-dimensional mathematical model based on the Method of Characteristics. It formulates valve closure strategies on the basis of existing maintenance measures and investigates hydraulic fluctuations under both gravity flow and pressurized water supply modes to elucidate the influence of air valves on the hydraulic transition process of water pipelines. The main conclusions drawn are as follows:

1. The study confirms the impossibility of simultaneous gravity and forced pump operation due to the excessive head provided by the pumps, which precludes the coexistence of both modes. Moreover, the pipeline exhibits a high surplus head under both supply modes, indicating its capability for long-term stable water supply.
2. Under gravity flow mode, a valve closure time of 30 s still meets the requirements of design specifications. Additionally, due to the density difference between water and air, gases mainly move upstream, leading to significant fluctuations in hydraulic parameters of upstream pipelines.

3. Under pressurized water supply mode, the first two and last valves of the water pipeline can still achieve the same hydraulic conditions as those obtained when all valves are closed for 60 s. However, due to the limited exhaust capacity of air valves, further extension of valve closure time does not yield significant benefits.

Author Contributions: Methodology, X.Z.; Software, Y.W.; Resources, Y.R.; Data curation, X.G. and T.W.; Writing—original draft, S.L. All authors have read and agreed to the published version of the manuscript.

Funding: The writers gratefully acknowledge the financial support: Three bidding sections of the scientific research service project of the river diversion project (Henan section) [grant numbers HNYJJH/JS/FWKY-2021003], and the National Key R&D Program of China [grant numbers 2022YFC3202504].

Data Availability Statement: The data that support the findings of this study are available from the corresponding author upon reasonable request.

Conflicts of Interest: Author Yongzhi Wang was employed by the Henan Water Diversion Engineering Co., Ltd. Author Tao Wang was employed by the Henan Water Diversion Engineering Co., Ltd. Author Yunlong Ran was employed by the Henan Water Valley Innovation Technology Research Institute Co., Ltd. The remaining authors declare that the research was conducted in the absence of any commercial or financial relationships that could be construed as a potential conflict of interest.

References

1. Liu, Y.; Pan, B.; Zhu, X.; Zhao, X.; Sun, H.; He, H.; Jiang, W. Patterns of microbial communities and their relationships with water quality in a large-scale water transfer system. *J. Environ. Manag.* **2022**, *319*, 115678. [[CrossRef](#)] [[PubMed](#)]
2. Zhang, Y.; Zhao, R.; Wang, H.; Peng, T.; Zhao, H. A Gateway to Rapid Prediction of Water Quality: A Case Study in China's South-to-North Water Diversion Project. *Water* **2021**, *13*, 2407. [[CrossRef](#)]
3. Zhou, Y.; Guo, S.; Hong, X.; Chang, F.-J. Systematic impact assessment on inter-basin water transfer projects of the Hanjiang River Basin in China. *J. Hydrol.* **2017**, *553*, 584–595. [[CrossRef](#)]
4. Zhou, L.; Feng, R.L.; Pan, T.; Li, Y.; Liu, D.; Che, T.-C. Coupled Second-Order GTS-MOC Scheme for Transient Pipe Flows with an Entrapped Air Pocket. *J. Hydraul. Eng.* **2023**, *149*, 04023030. [[CrossRef](#)]
5. Pan, T.; Zhou, L.; Ou, C.; Wang, P.; Liu, D. Smoothed particle hydrodynamics with unsteady friction model for water hammer pipe flow. *J. Hydraul. Eng.* **2022**, *148*, 04021057. [[CrossRef](#)]
6. Voordouw, G. Production-related petroleum microbiology: Progress and prospects. *Curr. Opin. Biotechnol.* **2011**, *22*, 401–405. [[CrossRef](#)] [[PubMed](#)]
7. Pan, B.; Keramat, A.; Duan, H.F. Energy Analysis for Transient-Leak Interaction and Implication to Leak Detection in Water Pipeline Systems. *J. Hydraul. Eng.* **2023**, *149*, 04023031. [[CrossRef](#)]
8. Brunone, B.; Maietta, F.; Capponi, C.; Duan, H.-F.; Meniconi, S. Detection of partial blockages in pressurized pipes by transient tests: A review of the physical experiments. *Fluids* **2023**, *8*, 19. [[CrossRef](#)]
9. Tee, K.F.; Wordu, A.H. Burst strength analysis of pressurized steel pipelines with corrosion and gouge defects. *Eng. Fail. Anal.* **2020**, *108*, 104347. [[CrossRef](#)]
10. Joukowski, N.E. Memoirs of the imperial academy society of St. Petersburg. *Proc. Am. Water Work. Assoc.* **1898**, *24*, 341–424.
11. Budinski, L. Application of the LBM with adaptive grid on water hammer simulation. *J. Hydroinform.* **2016**, *18*, 687–701. [[CrossRef](#)]
12. Ye, X.; Wang, Y.; Xie, Z.; Huang, M. Simulation of the Entire Process of an Interbasin Water Transfer Project for Flow Routing. *Water* **2024**, *16*, 572. [[CrossRef](#)]
13. Li, S.X.; Lou, Y.P.; Xu, X.G.; Ding, Q. Study on Water Hammer Suppression of Pipeline in Opening Process of Ultra-supercritical Steam Trap. *Fluid Mach.* **2016**, *44*, 24–28+86. (In Chinese) [[CrossRef](#)]
14. Zhu, M.; Zhang, X.; Zhang, Y.; Wang, T. Study on water hammer prevention in pump water supply systems by multi-valves. In Proceedings of the 2006 International Conference on Hybrid Information Technology, Cheju Island, Republic of Korea, 9–11 November 2006; Volume 1, pp. 342–346.
15. Kandil, M.; Kamal, A.M.; El-Sayed, T.A. Effect of pipematerials on water hammer. *Int. J. Press. Vessel. Pip.* **2020**, *179*, 103996. [[CrossRef](#)]
16. Hwang, Y.H. Development of a characteristic particle method for water hammer simulation. *J. Hydraul. Eng.* **2013**, *139*, 1175–1192. [[CrossRef](#)]
17. Liang, J.J.; Liu, H.X.; He, Q.; Gu, L. Establishment and analysis of water hammer prevention system in high-lift and long-distance water delivery system. *Fresenius Environ. Bull.* **2012**, *21*, 3659–3665.
18. Wang, C.; Yang, J.D. Water hammer simulation using explicit–implicit coupling methods. *J. Hydraul. Eng.* **2015**, *141*, 04014086. [[CrossRef](#)]

19. Riasi, A.; Nourbakhsh, A.; Raisee, M. Unsteady velocity profiles in laminar and turbulent water hammer flows. *J. Fluids Eng.* **2009**, *131*, 121202. [[CrossRef](#)]
20. Geng, J.; Yuan, X.; Li, D.; Du, G.-S. Simulation of cavitation induced by water hammer. *J. Hydrodyn.* **2017**, *29*, 972–978. [[CrossRef](#)]
21. Lu, M.; Liu, X.; Xu, G.; Tian, Y. Optimal pump-valve coupling operation strategy of complex long-distance water-conveyance systems based on MOC. *Ain Shams Eng. J.* **2024**, *15*, 102318. [[CrossRef](#)]
22. Zhang, X.; Bian, S.; Wang, H.; Jia, X.; Wang, C. Effects of valve opening on direct water hammer pressure characteristics in PMMA pipelines. *J. Braz. Soc. Mech. Sci. Eng.* **2023**, *45*, 408. [[CrossRef](#)]
23. Taieb, L.H.; Guidara, M.A.; Beltaieb, N.; El Aoud, S.; Taieb, E.H. Water-hammer control in an actual branched cast iron network by means of polymeric pipes. In *Advances in Acoustics and Vibration II: Proceedings of the Second International Conference on Acoustics and Vibration (ICAV2018), Hammamet, Tunisia, 19–21 March 2018*; Springer International Publishing: Cham, Switzerland, 2019; pp. 235–244.
24. Chang, Y.-T.; Yu, X.; Zhang, J.; Chen, X.-Y.; Chen, N.; Shi, L. Negative pressure protection with one-way surge tanks in bidirectional water delivery systems. *Water Supply* **2024**, *24*, 1089–1101. [[CrossRef](#)]
25. Lyu, J.; Zhang, J.; Wang, X.; Xu, T. A combined water hammer protective method for optimizing the volume of the air vessel in water supply systems. *AQUA—Water Infrastruct. Ecosyst. Soc.* **2021**, *70*, 1217–1230. [[CrossRef](#)]
26. Tasca, E.; Besharat, M.; Ramos, H.M.; Luvizotto, E.; Karney, B. Exploring the Sensitivity of the Transient Response following Power Failure to Air Valve and Pipeline Characteristics. *Water* **2023**, *15*, 3476. [[CrossRef](#)]
27. Wang, Y.; Zhang, J.; Xu, T.; Liu, Y.; Yao, T.; Wang, K.; Zhang, M. Air valve arrangement criteria for preventing secondary pipe bursts in long-distance gravitational water supply systems. *AQUA—Water Infrastruct. Ecosyst. Soc.* **2023**, *72*, 1566–1581. [[CrossRef](#)]
28. Li, X.; Wang, T.; Zhang, Y.; Guo, P. Study on the factors influencing air valve protection against water hammer with column separation and rejoinder. *AQUA—Water Infrastruct. Ecosyst. Soc.* **2022**, *71*, 949–962. [[CrossRef](#)]
29. Li, X.; Yan, T.; Bi, X.; Fei, L. Influence of traditional and antislam air valve characteristics on transient pressure control. *J. Pipeline Syst. Eng. Pract.* **2022**, *13*, 04022022. [[CrossRef](#)]
30. Bostan, M.; Akhtari, A.A.; Bonakdari, H.; Jalili, F. Optimal design for shock damper with genetic algorithm to control water hammer effects in complex water distribution systems. *Water Resour. Manag.* **2019**, *33*, 1665–1681. [[CrossRef](#)]
31. Alhwij, M.S.; Nakhleh, W. Optimal parameters of protection devices for controlling hydraulic transient using genetic algorithms. *AQUA—Water Infrastruct. Ecosyst. Soc.* **2024**, *73*, 623–636. [[CrossRef](#)]
32. Afshar, M.H.; Rohani, M. Water hammer simulation by implicit method of characteristic. *Int. J. Press. Vessel. Pip.* **2008**, *85*, 851–859. [[CrossRef](#)]
33. Zuo, Q.; Qiu, S.; Lu, W.; Tian, W.; Su, G.; Xiao, Z. Water hammer characteristics of integral pressurized water reactor primary loop. *Nucl. Eng. Des.* **2013**, *261*, 165–173. [[CrossRef](#)]
34. Pal, S.; Hanmaiahgari, P.R.; Karney, B.W. An overview of the numerical approaches to water hammer modelling: The ongoing quest for practical and accurate numerical approaches. *Water* **2021**, *13*, 1597. [[CrossRef](#)]
35. Finnemore, E.J.; Franzini, J.B. *Fluid Mechanics With Engineering Applications*; McGraw-Hill: New York, NY, USA, 2001.
36. Wang, L.; Wang, F.J.; Huang, J.; Luo, J.; Gui, X.; Xie, A. Filling transient analysis in pipelines with air valves. *J. Hydraul. Eng.* **2017**, *48*, 1240–1249. (In Chinese) [[CrossRef](#)]
37. Wan, W.; Huang, W. Investigation on complete characteristics and hydraulic transient of centrifugal pump. *J. Mech. Sci. Technol.* **2011**, *25*, 2583–2590. [[CrossRef](#)]
38. Yang, S.; Wu, D.; Lai, Z.; Du, T. Three-dimensional computational fluid dynamics simulation of valve-induced water hammer. *Proc. Inst. Mech. Eng. Part C J. Mech. Eng. Sci.* **2017**, *231*, 2263–2274. [[CrossRef](#)]
39. Sha, Y.; Wang, C.L.; Liu, T.; Shao, Z.; Weng, J. Measurement and hydraulic calculation of water hammer wave in pipe flow. *J. Exp. Mech.* **2007**, *22*, 527–533. [[CrossRef](#)]
40. Zhang, X.; Yin, Q.; Liu, F.; Li, H.; Qi, Y. Comparative study of rainfall prediction based on different decomposition methods of V.M.D. *Sci. Rep.* **2023**, *13*, 20127. [[CrossRef](#)] [[PubMed](#)]
41. Coelho, F.M.; de Azevedo, J.P.S. Design criteria for roughness values under real sewer system operating conditions. *J. Pipeline Syst. Eng. Pract.* **2022**, *13*, 04022018. [[CrossRef](#)]
42. Wang, K.L.; Zhang, J.; Yao, T.Y.; Wang, Y. Study on Water Hammer Protection of Long-distance Pressurized Gravity Flow Water Conveyance Project. *Water Resour. Power* **2023**, *41*, 76–80. (In Chinese) [[CrossRef](#)]

Disclaimer/Publisher’s Note: The statements, opinions and data contained in all publications are solely those of the individual author(s) and contributor(s) and not of MDPI and/or the editor(s). MDPI and/or the editor(s) disclaim responsibility for any injury to people or property resulting from any ideas, methods, instructions or products referred to in the content.